Sound & Vibration 2026, 60(2), 3856.
doi: https://doi.org/10.59400/sv3856

Article

Configuration and fault location method for network with limited traveling wave recorder based on hypothetical fault

Yongqi Liu[1], Jianbo Nie[1,2], Luyao Xie[1,*], Chao Zhu[3], Youbing Zhang[1]

[1] College of Information Engineering, Zhejiang University of Technology, Hangzhou 310014, China
[2] State Grid Zhejiang Comprehensive Energy Service Co., Ltd., Hangzhou 310016, China
[3] Economic and Technological Research Institute, State Grid Zhejiang Electric Power Co., Ltd., Hangzhou 310016, China
*** Corresponding author:** Luyao Xie, xieluyao@zjut.edu.cn

CITATION

Liu Y, Nie J, Xie L, et al. Configuration and fault location method for network with limited traveling wave recorder based on hypothetical fault. Sound & Vibration. 2026; 60(2): 3856. https://doi.org/10.59400/sv3856

ARTICLE INFO

Received: 9 December 2025
Revised: 5 February 2026
Accepted: 5 March 2026
Available online: 13 March 2026

Abstract: Fault location is crucial for enhancing power supply reliability and shortening power outage duration. Traditional power frequency-based fault location methods are limited by the distributed generation integration and the complex grid topology of renewable energy systems, while traveling wave (TW) fault location technology has become a research hotspot due to its high accuracy and fast response. The mainstream TW methods (single-ended, double-ended) have inherent drawbacks. This paper proposes a hypothetical fault-based fault location method: Acquire data from each sensor, obtain the time information of wavefronts via the db6 wavelet transform, and then construct a time matrix accordingly. Randomly assume a fault point, calculate the TW arrival time difference matrix between the hypothetical fault (based on shortest-path propagation) and the actual fault, derive the time information difference degree by comparing the two matrices, and iteratively update the hypothetical fault point via an optimization algorithm until the matrices coincide. Meanwhile, based on the hypothetical fault method, the mathematical expressions for the line fault observability constraints are derived, the optimal configuration model of traveling wave recorders in the network is established, and the solution is completed. This method achieves accurate fault location, assists in judging whether the network is measurable, and further enables the design of a planning and configuration model to realize the optimal configuration of TWRs under the condition of full-network fault observability without analyzing and deconstructing the network structure. Simulations are conducted on the IEEE 30-bus and IEEE 57-bus systems, respectively, to verify the method's effectiveness.

Keywords: fault location; wavelet transform; optimal configuration; traveling wave; wide-area synchronized measurements

1. Introduction

Fault location in power systems is crucial for enhancing power supply reliability and reducing power outage duration [1]. Traditional fault location methods based on power frequency quantities are susceptible to the impacts of factors such as transition resistance, distributed generation integration, and complex grid topology [2]. Traveling wave (TW) fault location technology has emerged as a research hotspot in the field of power system fault location due to its high accuracy and fast response capability [3]. This technology detects the TW signals generated upon the occurrence of faults and determines the fault point location based on the propagation time or characteristic differences of TW, thereby circumventing some limitations of traditional methods [4].

Three mainstream technical approaches are currently available for TW-based fault location, namely the single-ended method [5, 6], double-ended method [7, 8], and network location method [9, 10]. The single-ended method features a straightforward implementation framework, as it only leverages fault-related signals acquired from a single-terminal device; its core advantages include the elimination of clock synchronization requirements and reduced capital investment for system deployment. However, a key drawback of this method lies in its poor performance in identifying reflected waves generated by faults when applied to networks with intricate connection structures. In contrast, the double-ended method only relies on the arrival time of the initial traveling wave head for fault location, making it the most effective method applied in this field. Nevertheless, the double-ended method suffers from distinct limitations in certain practical scenarios. First, its fault positioning accuracy is highly susceptible to the rationality of traveling wave velocity selection, and an inappropriate wave velocity setting will directly induce a notable decline in location precision. In addition, the mandatory requirement of deploying location devices at both terminals of each transmission line gives rise to a substantial increase in equipment procurement, installation, and maintenance costs, which imposes economic pressure on the grid.

In actual power grids, especially in distribution networks and rural power grids featuring complex structures and numerous branches, they are confronted with multiple challenges [11]. Equipment commonly found in these networks, such as capacitor banks, voltage regulators, and transformers, may lead to the distortion and attenuation of TW signals [12]. Meanwhile, TW protection schemes require a high sampling frequency to accurately detect traveling wave fronts [13]. Existing TW fault location methods usually rely on installing detection equipment at all line terminals or key nodes, which not only increases economic costs but also brings inconvenience to equipment installation and maintenance [14]. For example, in MTDC grids, boundary components may not be available at the terminals of transmission lines, rendering traditional TW protection schemes inapplicable [15].

To address these challenges, researchers are actively exploring the use of fewer or more intelligent TWRs and improving the accuracy and robustness of fault location through advanced signal processing technologies, optimization algorithms, and data fusion methods. Yu et al. [16] have proposed a double-terminal TW fault location method based on frequency-dependent electrical parameters to enhance the fault location accuracy of high-voltage alternating current (HVAC) cable lines. Naidu and Pradhan [17] have proposed a novel double-terminal TW fault location method, which combines the advantages of the single-terminal method and the double-terminal method to resolve the demand for strict clock synchronization in traditional double-terminal methods and the deficiencies of single-terminal methods in wave velocity accuracy and wave front identification. To address the issues of clock synchronization errors and inaccurate TW velocity in TW network location methods, Wu et al. [18] have proposed a TW network location method based on virtual fault time difference information, which improves positioning accuracy by simulating the TW propagation of virtual faults. Zhang et al. [19] analyzed and decoupled the information of fault distance and fault severity, realizing rapid fault location. Xia et al. [20] proposed a multi-fault

location method based on virtual faults, achieving the simultaneous high-precision location of multiple fault points. Xia et al. [21] optimized and calibrated traveling wave wavefronts, addressing the time calibration issue of weak fault signals in fault location. These network-based fault location methods have often been proven effective in networks equipped with far more sensors than the required quantity.

Considering the installation cost of a traveling wave recorder (TWR), it is important to investigate the placement scheme of the fault detectors at minimal locations on the network so that the fault location can be observability achieved over the entire network. Galvez and Abur [22] investigated how to achieve fault location on sparse TWR datasets and proposed a TWR configuration method to ensure network observability, but it fails to achieve the minimum number of TWRs. Salehi et al. [23] obtained the TWR configuration scheme by analyzing and deconstructing the network structure. Mohammadi et al. [24] realized the optimal configuration under full-network fault observability through sensitivity analysis; however, it requires additional voltage and current information and is mainly oriented toward phasor measurement units (PMUs) rather than TWRs. Dolatabadi and Golshan [25] analyzed the observability of impedance-based fault location, yet did not formulate such observability as constraints or solve the corresponding problem in sensor configuration planning. Mohammadniaei et al. [26] implemented fault location with a small number of sensors in simple networks based on game theory and the Dijkstra algorithm, but this method is hardly applicable to complex networks such as ring networks. Maritz et al. [27] used the concepts of metric dimension and vertex covers in a graph to achieve the optimal quantity and placement of detectors. This approach first determines the minimum number of detectors via network analysis and then realizes optimal deployment through a placement algorithm. This paper will propose a one-step method.

This paper proposes a fault location method based on hypothetical faults, which can achieve accurate fault location, assist in judging whether the network is measurable, and further design a planning and configuration model to realize the optimal configuration of TWRs under the condition of full-network fault observability without analyzing and deconstructing the network structure.

2. Traveling wave location method based on hypothetical faults

Consider *m* TWRs deployed in the network, each capturing the time of arrival (ToA) of fault-originated traveling waves, which jointly constitute the dataset T_m.

$$T_m = (t_1, t_2, \cdots, t_k, \cdots, t_m)^T \tag{1}$$

For a power grid with *N* nodes and *L* lines. A scale coefficient $\tau \in [0, 1]$ is introduced to represent the distance from the fault point to the head end of the line, where $\tau = 0$ and $\tau = 1$ correspond to the bus fault cases. The propagation time (i.e., delay) from the fault occurrence point to the sensor depends on the network topology, propagation velocity, as well as three unknown variables [28]:

1) the identity of the faulty line (a, b);
2) the location of the fault on the line ($\tau \in [0, 1]$);

3) the time instant at which the fault has occurred (t_0).

Obviously, for the *k*-th TWR, a corresponding equation exists. This dataset yields an overdetermined system of equations. The contributions of the hypothetical fault method proposed in this paper are as follows:

1) It can accurately obtain the unique solution when the number of measurement points *m* is less than the total number of nodes *N* and the system of equations has a unique solution, thus achieving precise fault location.
2) It can assist in judging whether the current TWR installation scheme of the network can realize full-network fault observability.
3) It further presents an optimal configuration method to achieve full-network fault observability with the minimum number of installed TWRs.

2.1. Fault traveling wave arrival time function based on Dijkstra algorithm

A grid can be modeled as a graph structure, where arcs denote transmission lines and nodes represent buses. When a fault occurs on a transmission line, a transient waveform is generated and propagates throughout the network. The Dijkstra algorithm is a classic algorithm for solving the shortest path problem between any two nodes in a network structure [29]. We construct a weighted matrix V by taking the line length and the wave velocity correction coefficient as the weights.

$$V = \begin{bmatrix} V_{11} & V_{12} & \cdots & V_{1n} \\ V_{21} & V_{22} & \cdots & V_{2n} \\ \vdots & \vdots & \ddots & \vdots \\ V_{n1} & V_{n2} & \cdots & V_{nn} \end{bmatrix} \tag{2}$$

$$V_{ij} = \begin{cases} v_{ij}^{'} l_{ij} & \text{node } i,j \text{ connected} \\ \infty & \text{node } i,j \text{ not connected} \\ 0 & i = j \end{cases} \tag{3}$$

$v_{ij}^{'}$ refers to the wave velocity correction coefficient, which is applied when there are significant differences in the wave velocities of lines in the network, and it is generally set to 1. Based on the weighted matrix, the shortest path between node *i* and node *j* can be calculated by the Dijkstra algorithm, denoted as d_{ij}.

Therefore, the shortest path of the fault TW from the fault point f on line l_{ab} to the *i*-th node in the system can be expressed as

$$d_{fi} = min\left\{\tau l_{ab} + d_{ai}, (1-\tau) l_{ab} + d_{bi}\right\} \tag{4}$$

thus,

$$t_i - t_0 = d_{fi} \cdot \frac{1}{v} \tag{5}$$

By subtracting the arrival times of the initial fault TW pairwise, the fault

occurrence time t_0 can be eliminated.

$$t_{ij} = t_i - t_j = \frac{1}{v}(min\{\tau l_{ab} + d_{ai}, (1-\tau)l_{ab} + d_{bi}\} - min\{\tau l_{ab} + d_{aj}, (1-\tau)l_{ab} + d_{bj}\}) \tag{6}$$

t_{ij} is evident that the function is a piecewise function of τ, and its graph can be plotted as shown in **Figure 1**. Since the relative positions of the breakpoints and the value range of [1] on the coordinate axis depend on the network structure, the graph of the function over the interval [1] may take various forms, including a constant function, a linear function, a two-segment piecewise function, or a three-segment piecewise function.

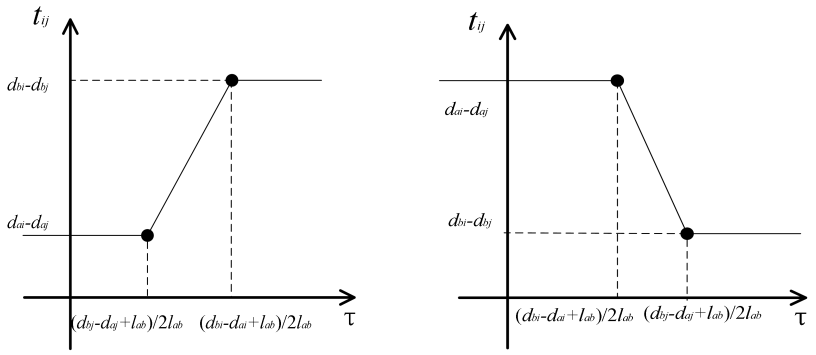

Figure 1. Different cases of the two piecewise functions: **(a)** when $(d_{bj} - d_{aj} + l_{ab})/2l_{ab} < (d_{bi} - d_{ai} + l_{ab})/2l_{ab}$; **(b)** when $(d_{bj} - d_{aj} + l_{ab})/2l_{ab} \geq (d_{bi} - d_{ai} + l_{ab})/2l_{ab}$.

Solve for τ corresponding to all branches to obtain the solution set; the intersection of all solution sets is the desired fault point. It is not difficult to see that the complexity of the above method lies in the fact that multiple points are often obtained when solving for the fault points that satisfy the known time difference relationship, which requires repeated classified discussions during the solution process. In addition, this method is quite sensitive to parameters such as wave velocity and wave velocity correction coefficient.

2.2. Overall idea and process of hypothetical fault

When the line number and scale coefficient are known, the forward calculation of time differences is much more convenient compared with the above method. Based on this idea, this paper proposes a fault location method based on hypothetical faults, and its overall operation process is as follows:

The fault localization method randomly assumes a hypothetical fault point in the transmission line. Based on the shortest-path propagation characteristic of the initial fault TW, it calculates the time difference matrix of the initial TW from the hypothetical fault arriving at all measurement points. The accuracy of the hypothetical fault point's location is measured by the time information difference degree between the hypothetical fault and the actual fault. The hypothetical fault point's location is continuously updated in an optimized manner to approach the actual fault point. The localization process is as follows:

1) After a fault occurs in the transmission line, the initial fault TW reaches each substation along the shortest path. The arrival time of the initial TW is recorded by the TW detection device. The arrival times of the initial TW at all measurement points are subtracted pairwise to obtain the time difference matrix of the actual fault.
2) Multiple points are randomly selected as hypothetical fault points in the transmission line. The initial fault TW signal is sequentially simulated to propagate to each measurement point along the shortest path. The arrival time of the initial TW from the hypothetical fault point at each measurement point is calculated based on the TW velocity and propagation path length of the hypothetical fault, and then the time differences are computed pairwise to obtain the time difference matrix of the hypothetical fault.
3) The time information difference degree is derived by comparing the time difference matrix of the actual fault with that of the hypothetical fault.

Select an optimization algorithm to update the position of the hypothetical fault point, and repeat Steps 2) and 3) to gradually approach the actual fault point. Only when the hypothetical fault point coincides with the actual fault point do their time difference matrices show consistency, with all elements in the matrices fully matching and the time information difference degree equal to 0.

2.3. Calculation of time difference matrix and time information difference degree

The arrival times of the initial fault TW are subtracted pairwise to obtain the time difference matrix ΔT_m of the actual fault. Since ΔT_m is a skew-symmetric matrix, the lower triangular part is set to zero.

$$\Delta T_m = \begin{bmatrix} 0 & t_{12} & \cdots & t_{1m} \\ 0 & 0 & \cdots & t_{2m} \\ \vdots & \vdots & \ddots & \vdots \\ 0 & 0 & \cdots & 0 \end{bmatrix} \tag{7}$$

To weaken the impact of factors such as wave velocity attenuation and time measurement error of remote measurement points on location accuracy, weights are assigned according to the fault distance. The longer the fault propagation distance to the two measurement points, the lower the weight of the time difference between these two points. The time information dissimilarity e_t is defined as the l-norm of the time information difference matrix, divided by the number of elements in the matrix to eliminate the influence of the TWR count.

$$e_t \overset{\text{def}}{=} \frac{1}{m(m-1)} \left\| \Delta \widehat{e} \right\|_l \tag{8}$$

$$\Delta \widehat{e} = \begin{bmatrix} 0 & \frac{t_{12}^{'} - t_{12}}{d_{f1} + d_{f2}} & \cdots & \frac{t_{1m}^{'} - t_{1m}}{d_{f1} + d_{fm}} \\ 0 & 0 & \cdots & \frac{t_{2m}^{'} - t_{2m}}{d_{f2} + d_{fm}} \\ \vdots & \vdots & \ddots & \vdots \\ 0 & 0 & \cdots & 0 \end{bmatrix} \tag{9}$$

The Particle Swarm Optimization (PSO) algorithm can be selected as the solution algorithm [30]. To ensure the speed and accuracy of fault location, this paper takes the minimization of the time information difference degree as the objective, takes the actual fault point position as the solution, and transforms this problem into a solution optimization problem. The fitness function is selected as the reciprocal of the time information difference degree, and more initial positions of particles are distributed on the lines where the nodes with earlier arrival times of the initial TW are located.

PSO starts with algorithm initiation and parameter initialization, during which the population size, maximum number of iterations, search space dimension, variable boundaries, the inertia weight, cognitive coefficient, and social coefficient are specified. After this initialization, the position and velocity vectors of all particles in the population are randomly generated to ensure they lie within the preset feasible search space.

Next, the fitness value of each particle's current position is calculated using Equation (8), serving as the metric to evaluate particle performance. Each particle's personal best position is initialized to its own starting position, while the global best position of the entire population is identified by traversing all particles and selecting the one with the optimal fitness. The iterative optimization loop then commences. Subsequently, particle positions are adjusted based on the updated velocities, and any out-of-bounds positions or velocities are corrected to the feasible domain using methods such as truncation or reflection. After updating positions, the new fitness value of each particle is recomputed. This iterative process continues until the termination criteria are met—including reaching the maximum number of iterations and fitness converging to a preset precision threshold.

The flowchart of the fault location method based on a hypothetical fault is shown in **Figure 2**.

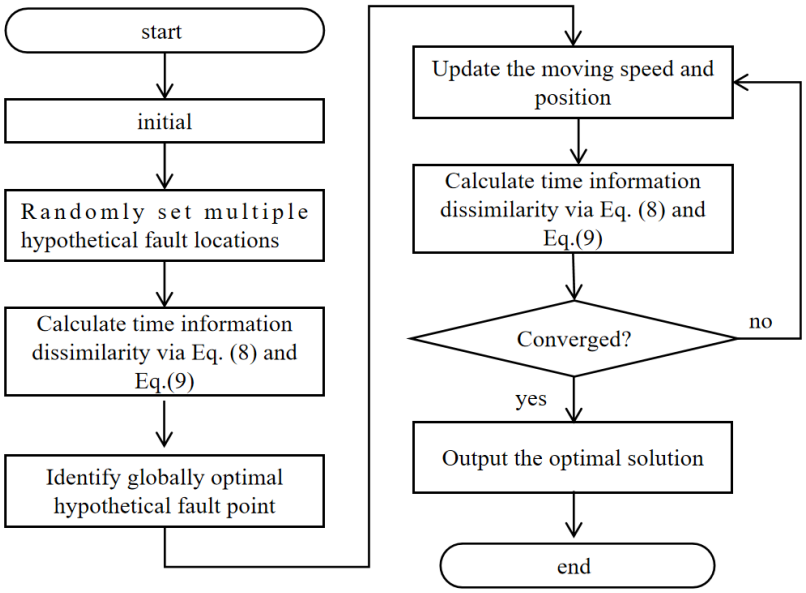

Figure 2. Flowchart of fault location method based on hypothetical fault.

In addition, the wave velocity information is actually included in the time

difference matrix. To eliminate the errors of parameters such as wave velocity error, the wave velocity can also be set as an unknown variable. The weighted matrix of the formula is modified according to the wave velocity ratio of the actual lines to increase the number of variables, thereby eliminating the impact of wave velocity.

2.4. Hypothetical fault-based TWR configuration method

To meet the requirement of minimizing the number of TWR deployments, and further considering the actual installation requirement degree of each node, the objective function, as shown in Equation (10), is established. Where x_k is the variable for configuring the TWR at node *k* (1 indicates configuration, and 0 indicates non-configuration), and w_k is the weight coefficient of the TWR installation requirement degree for node *k*. The calculation method of w_k is derived from Liang et al. [31].

$$\begin{aligned} &\min \sum_{N}^{k=1} w_k x_k \\ &x_k \in \{0,1\} \end{aligned} \tag{10}$$

Fault non-locatability means that the movement of the hypothetical fault point will not cause any change in the time difference relationship of any TWR, that is to say, the change in the time information difference degree, i.e.,

$$\frac{\partial e_t}{\partial \tau} = 0 \quad \forall l_{ij} \tag{11}$$

When the configuration scheme is still to be determined in the planning phase, the previous formula can be rewritten as the following formula. A TWR configuration variable is added before each term to indicate that the corresponding term in the time difference matrix is non-zero only when both nodes are equipped with TWRs.

$$\Delta\widehat{e} = \begin{bmatrix} 0 & x_1 \cdot x_2 \cdot \frac{t_{12}^{'} - t_{12}}{d_{f1}+d_{f2}} & \cdots & x_1 \cdot x_n \cdot \frac{t_{1n}^{'} - t_{1n}}{d_{f1}+d_{fn}} \\ 0 & 0 & \cdots & x_2 \cdot x_n \cdot \frac{t_{2n}^{'} - t_{2n}}{d_{f2}+d_{fn}} \\ \vdots & \vdots & \ddots & \vdots \\ 0 & 0 & \cdots & 0 \end{bmatrix} \tag{12}$$

$$m = \sum_{k=1}^{n} x_k \tag{13}$$

It can be seen from the analysis of the graph that as long as it is ensured that the piecewise function is not a constant near both 0 and 1 simultaneously, there will be at least one term changing in the time information difference degree matrix, and thus this line is measurable. Then, the condition to ensure the measurability of line *ij* can be expressed as the following formula. Full-network measurability can be achieved if the measurability condition is satisfied for all lines through traversal.

$$\frac{e_t \,|\tau = 0, f \in l_{ij} - e_t \,|\tau = 0 + \Delta\tau, f \in l_{ij}}{\Delta\tau} \neq 0 \tag{14}$$

$$\frac{e_t\,|\tau = 1, f \in l_{ij} - e_t\,|\tau = 1 - \Delta\tau, f \in l_{ij}}{\Delta\tau} \neq 0 \tag{15}$$

It is noted that the actual fault time difference matrix in the formula is a constant matrix, and $\Delta\tau$ is very small, so the actual fault time differences can be regarded as offsetting each other for the convenience of calculation. Combined with the formula, the 0–1 programming problem can be solved to obtain the configuration matrix.

The fast non-dominated sorting genetic algorithm (NSGA-II) is widely applied to problems whose objective function takes the form of the sum of coefficient-weighted 0–1 variables. The 0–1 coding characterizing the installation status of measurement devices is arranged in a sequence, whose structure is highly similar to the relationship between genes and chromosomes in genetic algorithms. The gene indices of the initial population correspond to the system node numbers, and the values of genes on the chromosome represent the traveling wave unit allocation status of the respective nodes.

This method satisfies constraints through the constraint-dominance criterion, with the judgment rules specified as follows: If both individuals are feasible solutions, the original Pareto dominance rule of NSGA-II is adopted directly for comparison; If one individual is feasible and the other is infeasible, the feasible solution is directly superior to the infeasible one; If both individuals are infeasible, the individual with a smaller constraint violation degree is deemed better.

After the initial population is determined, NSGA selects superior individuals on the basis of non-dominated sorting stratification, crowding distance calculation, and the elitist preservation strategy. A new population is generated through genetic operations, and the iterative cycle proceeds until the termination criterion is met.

The flow chart of this method is shown in **Figure 3**.

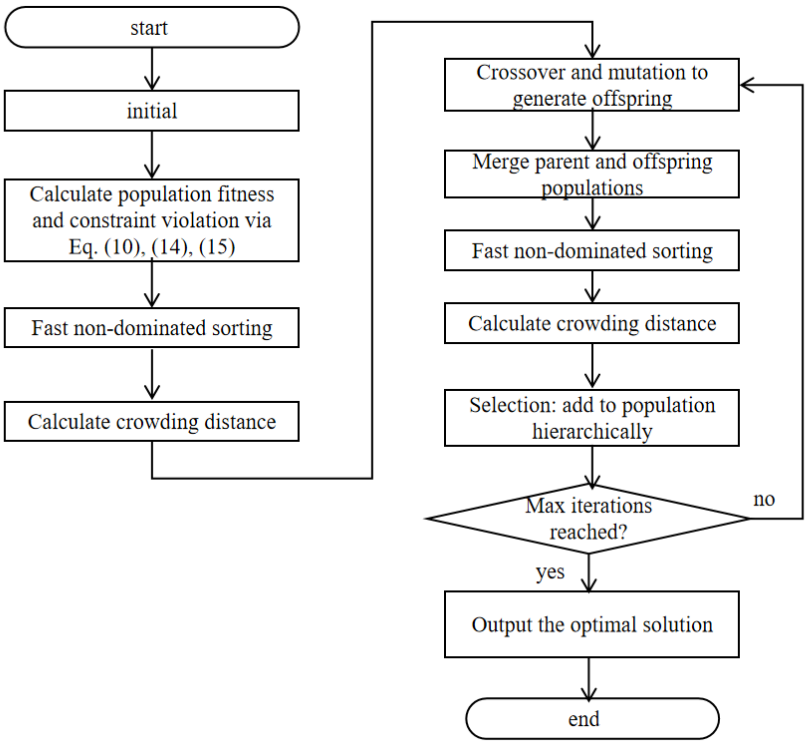

Figure 3. Flowchart of hypothetical fault-based TWR configuration method.

3. Results and discussion

3.1. Results of the TWR configuration scheme

The IEEE 30-bus system is illustrated in **Figure 4**, which consists of 57 transmission lines [32]. Utilizing the method described above, the configuration vector X is obtained as X = [1]. In this vector, elements with a value of 1 indicate the nodes where TWRs need to be installed, namely Nodes 2, 3, 5, 8, 11, 13, 14, 17, 19, 21, 26, 29, and 30. These nodes are marked by black solid circles in **Figure 4**.

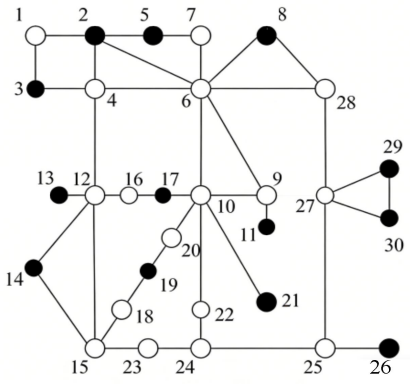

Figure 4. Single-line diagram of the IEEE 30-node test system.

The standard IEEE 57-bus system comprises 78 transmission lines [33]. Through calculation, the nodes requiring TWR configuration are determined as Nodes 3, 5, 16, 17, 21, 31, 33, 42, 43, 45, 46, 51, and 53, which are denoted by solid circles in **Figure 5**.

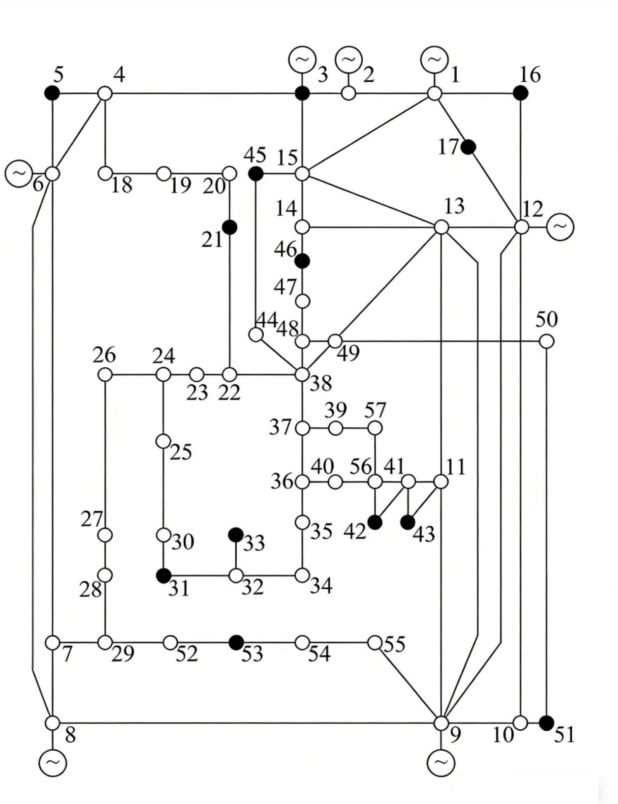

Figure 5. Single-line diagram of the IEEE 57-node test system.

Compared with the IEEE 30-bus power system, the IEEE 57-bus system sees a 90% increase in the number of buses and a 36.8% growth in the number of lines. Nevertheless, only 13 buses need to be equipped with traveling wave recorders (TWRs), which is equivalent to the configuration quantity of the IEEE 30-bus system. This indicates that remarkable cost savings can be realized for power grids while achieving full-network fault locatability, and further validates the effectiveness of the method proposed in this paper.

Reliability and economic efficiency constitute conflicting objectives. Monitoring a larger number of bus and line faults with an identical quantity of TWRs will inevitably result in degraded reliability. In the subsequent sections, the two schemes will be evaluated using the N-1 criterion.

Specifically, the N-1 criterion is a standard for judging the safety of power systems [33]. In practical applications, TWRs may malfunction, leading to data errors or loss, which increases the fault range in blind areas. Therefore, the N-1 analysis of power grids is adopted to improve the reliability of fault ranging.

The fault measurable degree is defined as the ratio of the length of measurable sections to the total length of system lines. If the fault measurable degree of the system decreases significantly after a certain TWR is out of service, failing to meet the requirements of practical engineering, a small number of additional configuration points need to be added to enhance the system reliability. Meanwhile, the redundancy of the system increases, and the economy of the configuration decreases.

It is assumed that the engineering requirement specifies that the fault measurable degree should reach more than 95% after one TWR is out of service. The unmeasurable sections (expressed as a proportion) and measurable degrees under the N-1 condition are calculated by withdrawing each configured node separately, as shown in **Table 1**.

Table 1. The degree of observability for the IEEE 30-node system.

N-1 node	Unmeasurable sections	Fault measurable degree (%)
2	2-4 2-6	99.2
3	1-3 1-2 3-4	98.1
5	2-5 6-7	99.8
8	7-8 8-28	95.6
11	6-9 9-11 9-10	97.0
13	12-13	99.7
14	12-14 14-15	98.3
17	10-17 12-16	99.0
19	10-20 12-15 15-18 19-20	98.2
21	10-21 21-22	98.7
26	10-22 25-26	97.7
29	27-29 29-30	97.0
30	27-30 29-30	99.4

For the solution of the IEEE 30-bus system, evidently, when the device at any node is out of service, the fault measurable degree is higher than 95%, meeting the engineering requirements. However, the conclusion differs completely when the same method is adopted for the IEEE 57-bus system, as shown in **Table 2**.

Table 2. The degree of observability for the IEEE 57-node system

N-1 node	Number of unmeasurable sections	Length of unmeasurable sections (km)	Fault measurable degree (%)
3	10	820.5	94.2
5	8	493	96.5
16	9	722	94.9
17	8	701.5	95.1
21	9	880	93.8
31	8	399.5	97.2
33	7	424	97.0
42	8	682	95.2
43	8	410	97.1
45	8	506	96.4
46	12	1,330	90.6
51	11	1,141	92.0
53	11	1,176	91.7

When certain critical nodes in the power network are rendered out of service due to equipment maintenance, accidental faults, or operational scheduling, the overall system fault measurable degree drops to below 95%, which directly fails to satisfy the strict technical indicators and practical engineering requirements for power grid fault location. It is a theoretically reasonable and practically common phenomenon that the system's N-1 reliability experiences a corresponding decline when the same number of TWR units are assigned to monitor a larger number of transmission lines. This is because the monitoring load borne by each TWR increases significantly, and the redundant measurement coverage of the network is compressed, leading to a natural reduction in the fault measurable degree under contingency conditions.

To address this reliability degradation issue and bring the system performance back into compliance with engineering standards, a targeted iterative optimization strategy can be adopted. Specifically, the N-1 nodes that suffer a substantial drop in fault measurability can be defined as mandatory installation nodes and set to 1 in the constraint conditions of the allocation model. On this basis, the total number of TWR configurations is increased by one unit, and the optimal allocation model is re-run and recalculated. This cyclic constraint adjustment and re-optimization process is repeated continuously until the fault measurable degree meets the predefined engineering requirements.

The detailed calculation results summarized in **Table 3** fully validate the effectiveness of this improved strategy: the deployment of 18 TWRs can not only meet the mandatory engineering requirements for fault measurable degree and N-1 reliability but also maintain a high level of economic efficiency in terms of equipment investment and grid operation costs.

In addition, for practical engineering projects that place a higher priority on the economic efficiency of TWR allocation and have strict cost control constraints, the threshold requirement for the N-1 fault measurable degree can be appropriately relaxed within a technically feasible range. This flexible adjustment can effectively reduce the number of additional nodes requiring TWR configuration, enabling a customizable trade-off between system reliability and deployment economy to adapt to diverse

engineering application scenarios and planning objectives.

Table 3. The degree of observability for the IEEE 57-node system after recalculation.

N-1 node	Length of unmeasurable sections (km)	Fault measurable degree (%)
3	307	97.8
5	493	96.5
14	307	97.8
16	675	95.2
17	672	95.3
19	307	97.8
21	307	97.8
31	330	97.7
33	424	97.0
42	682	95.2
43	410	97.1
45	506	96.4
46	307	97.8
47	307	97.8
50	307	97.8
51	561.5	96.0
52	307	97.8
54	307	97.8

3.2. Analysis of fault location methods

The IEEE 30-bus system in Section 3.1 is established on PSCAD/EMTDC for real-time detection of fault traveling waves. After phase-mode transformation, the line-mode TWs are utilized for wave front detection, and the arrival time of the initial TWs is recorded. The sampling frequency is set to 1 MHz, and the clock precision is set to 10 ns.

First, in the field of power system fault traveling wave analysis, the three-phase voltage traveling waves excited by actual fault disturbances are decoupled through the Karenbauer transformation, which effectively uncouples the mutually coupled electrical quantities into independent line-mode and zero-mode components. Subsequently, the wavelet transform is introduced as a core signal processing tool to precisely calibrate the arrival time of traveling wave fronts. Among numerous candidate wavelet basis functions, the db6 wavelet transform outperforms other common wavelet transforms in two critical aspects: it exhibits superior time-domain locality for capturing transient abrupt signals and a higher degree of energy concentration for fault-induced traveling wave components, which effectively mitigates the attenuation effects of traveling wave signals during propagation. Given these prominent advantages, the db6 wavelet is specifically selected as the dedicated wavelet basis for conducting wavelet transform processing on both line-mode and zero-mode traveling wave waveforms in this paper. Meanwhile, the high-frequency decomposition part of the wavelet transform has a more significant effect on the detection of abrupt signals; thus, the 1st layer of the high-frequency decomposition part is used to calibrate the arrival time of line-mode and zero-mode wave fronts, with the results shown in **Figure 6**.

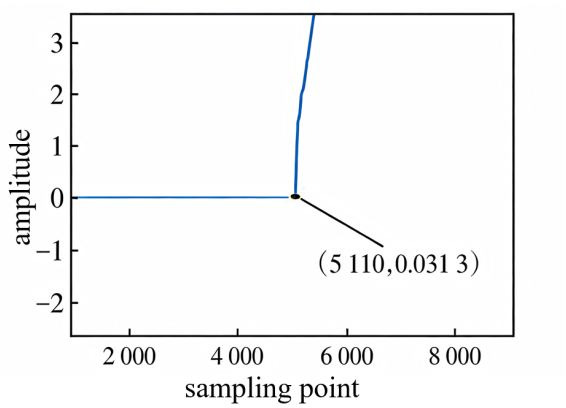

(a) Zero-mode waveform.

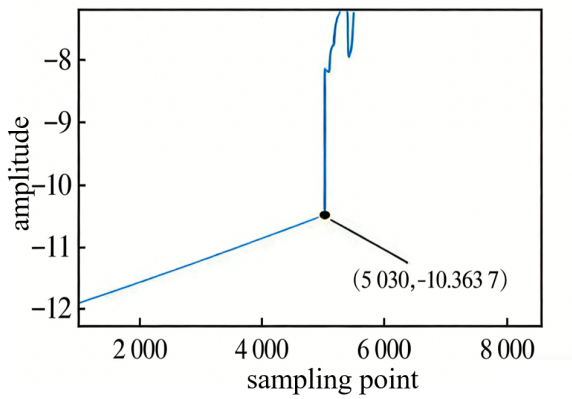

(b) Line-mode waveform.

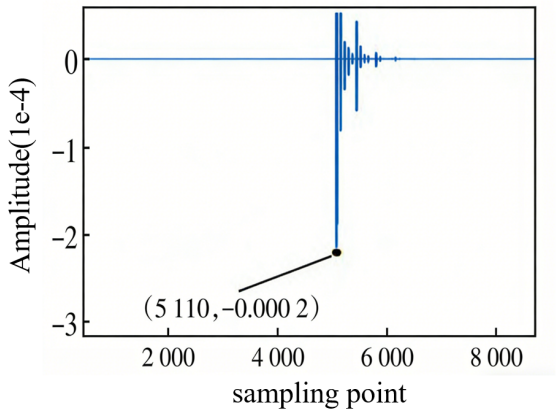

(c) Zero-mode wavelet decomposition.

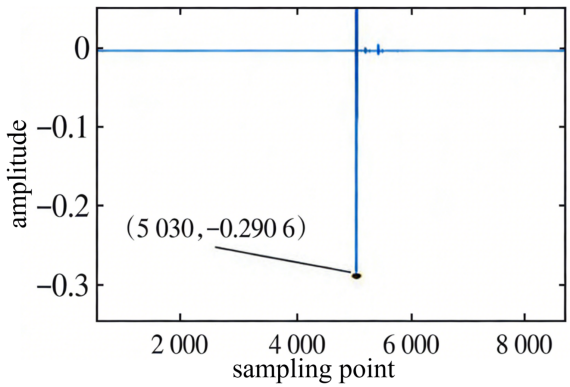

(d) Line-mode wavelet decomposition.

Figure 6. Calibration of the travelling wave line and zero-mode component wave head.

To comprehensively validate the fault location performance of the proposed method, a series of random faults is intentionally generated across different transmission lines in the test system, covering diversified fault locations and common fault scenarios in actual power grid operation. Partial representative results of the fault location tests are summarized in **Table 4**. Statistical analysis of the location outputs shows that the average fault location error is controlled at 59 m, and the maximum location error is merely 97 m. Such a low error level fully meets the strict precision requirements of practical power system fault location engineering, and it is evident that the proposed method presents outstanding and stable high-precision location performance.

In addition, to further quantitatively verify the optimization effect of the proposed algorithm on the TW velocity adopted for traveling wave fault location calculation, a typical Phase A-ground fault is set at a position 30 m away from the reference terminal on Line 6-9. On this basis, a set of comparative fault location calculations is carried out by employing a series of different traveling wave velocities as the core calculation parameter. The detailed location errors and corresponding analysis results under different traveling wave velocity conditions are specifically presented in **Table 5**.

Table 4. Partial random faults (fault location results).

	Line	Length (km)	Actual fault location (km)	Absolute error (m)
1	1-2	42	30	28
2	1-3	274	80	75
3	2-4	278	90	69
4	2-5	51	20	18
5	2-6	241	100	97
6	3-4	80	30	64
7	4-6	112	90	26
8	4-12	27	10	17
9	5-7	173	20	18
10	6-7	31	10	9

Table 5. Results of different simulations and calculation wave of velocity.

Simulation wave velocity (km/μs)	Calculation wave velocity (km/μs)	Absolute error (m)
0.2930	0.2927	57
	0.2930	26
	0.2933	83
	0.2947	102
	0.2950	107
	0.2953	109
	fitted wave velocity	28
0.2950	0.2927	132
	0.2930	134
	0.2933	130
	0.2947	43
	0.2950	25
	0.2953	77
	fitted wave velocity	32

The results clearly demonstrate that the selection of TW velocity serves as a pivotal factor exerting a significant impact on the precision of fault location calculation outcomes. Specifically, a distinct monotonic correlation is identified between the preset computational wave velocity and the absolute location error: the more closely the selected calculation wave velocity approximates the actual propagation velocity of fault-induced traveling waves along transmission lines, the smaller the corresponding absolute positioning error, which aligns with the fundamental theoretical mechanism of traveling wave fault location.

Notably, when the chosen TW velocity deviates substantially from the real-world propagation velocity, the absolute location error does not manifest a proportional amplification trend alongside the degree of velocity deviation. This favorable non-linear error characteristic arises because the inherent wave velocity information embedded within the time difference matrix constructed from the measurement data of remote TWRs exerts a critical constraining and compensating effect. Such implicit wave velocity-related features effectively suppress the uncontrolled propagation and accumulation of errors triggered by velocity mismatching, preventing excessive degradation of location accuracy.

Furthermore, when the TW velocity is additionally incorporated as an independent optimization variable into the integrated fault location model, the adverse interference caused by wave velocity uncertainty and deviation on the final location results can be significantly mitigated. This variable-setting strategy enables the model to adaptively match the actual traveling wave propagation velocity under diverse grid operating conditions and line parameters, further enhancing the robustness and fault tolerance of the proposed location method.

Additionally, the influence of the initial fault phase angle is also studied in this paper. A phase A ground fault is set 10 km away from Node 9 on Line 9-10, with 9 groups of fault phase angles ranging from 10° to 90°. The conclusions are shown in **Table 6**.

Table 6. Results of different fault initial phase angles.

Initial fault phase angle (°)	Absolute error(m)
90	35
80	24
70	68
60	59
50	66
40	76
30	89
20	68
10	81

Specifically, extensive experimental validation confirms that the proposed fault location method delivers superior high-precision positioning performance under large initial fault phase angle conditions. Although the location accuracy shows a slight decline when the initial fault phase angle is relatively small, the overall positioning error still stays within a satisfactory, engineering-qualified range and ensures reliable fault localization.

The intrinsic physical mechanism behind this phenomenon lies in the fact that the amplitude of the fault-induced TW is essentially dominated by the additional potential established at the fault point. When the initial phase angle of the fault voltage is small, the abrupt amplitude of the generated traveling wave is inherently weak. After suffering from unavoidable attenuation, waveform distortion, and electromagnetic interference during its propagation along the transmission line, the faint traveling wave front becomes significantly harder to accurately identify and extract by the deployed TWRs, which accounts for the mild reduction in location accuracy.

In general, regardless of the variations in initial fault phase angles—covering both small and large operating conditions—the fault location method proposed in this paper maintains favorable robustness and positioning precision, and is capable of realizing accurate and dependable fault location across different fault inception scenarios in practical power grid operations.

4. Conclusion

This paper proposes a fault location method based on hypothetical faults, which can achieve accurate fault location, assist in judging whether the network is measurable, and further design a planning and configuration model to realize the optimal configuration of TWRs under the condition of full-network fault observability.

During the analysis of the economy and reliability of configurations, the N-1 requirement is difficult to formulate directly as a constraint. Therefore, an approach was adopted that retains nodes with large unobservable areas after pruning and then increases the number of configured nodes. However, this method may not be optimal. Future research could explore ways to directly incorporate reliability constraints into the model.

When analyzing fault location methods, the accuracy of wavefront calibration is a key factor affecting positioning accuracy. In many cases, the increase in errors stems from the degradation of wavefront calibration accuracy. Future studies may focus on developing more precise wavefront calibration methods.

Author contributions: Conceptualization, JN; methodology, YL; software, YL; validation, LX and CZ; formal analysis, YZ; investigation, LX; resources, YZ; data curation, YL; writing—original draft preparation, YL; writing—review and editing, YL; visualization, LX; supervision, CZ; project administration, JN; funding acquisition, JN. All authors have read and agreed to the published version of the manuscript.

Funding: This work was supported by Zhejiang Electric Power Industry Corporation Technology Project (No. 5211JY260002) and National Natural Science Foundation of China (No. U22B20l16).

Institutional review board statement: Not applicable.

Informed consent statement: Not applicable.

Data availability statement: The basic data used in this study are obtained from other researchers, with corresponding citations in the main text.

Conflict of interest: The authors declare no conflict of interest.

References

1. Wang S, Xu G. Research on traveling wave fault technology based on ground potential. AIP Advances. 2021; 11(11): 115009. doi: 10.1063/5.0069963
2. Shu H, Liu H, Tang Y, et al. Fault Identification Method for Measured Travelling Wave of Transmission Line Based on CSCRFAM-Transformer. Protection and Control of Modern Power Systems. 2025; 10(2): 69–82. doi: 10.23919/PCMP.2023.000322
3. Xie Z, Li Bin, He J, et al. Hybrid HVDC system fault transient analysis considering traveling wave propagation and converter control response. International Journal of Electrical Power & Energy Systems. 2023; 147: 108794. doi: 10.1016/j.ijepes.2022.108794
4. Hong H, Cheng Z, Yang H, et al. Wave-Speed-Independent Traveling Wave Fault Location Method for Flexible DC Transmission Lines. Energies. 2025; 18(22): 5924. doi: 10.3390/en18225924
5. Naidu OD, Pradhan AK. Precise Traveling Wave-Based Transmission Line Fault Location Method Using Single-Ended Data. IEEE Transactions on Industrial Informatics. 2021; 17(8): 5197–5207. doi:

10.1109/TII.2020.3027584
6. Zhang C, Song G, Wang T, et al. Single-Ended Traveling Wave Fault Location Method in DC Transmission Line Based on Wave Front Information. IEEE Transactions on Power Delivery. 2019; 34(5): 2028–2038. doi: 10.1109/TPWRD.2019.2922654
7. Liu Y, Cao YD, Hou CG. The cable two-terminal fault location algorithm based on EMD and WVD. Proceedings of the CSEE. 2015; 35(16): 4086–4093. (in Chinese)
8. Abd el-Ghany HA, Azmy AM, Abeid AM. A General Travelling-Wave-Based Scheme for Locating Simultaneous Faults in Transmission Lines. IEEE Transactions on Power Delivery. 2020; 35(1): 130–139. doi: 10.1109/TPWRD.2019.2931178
9. Zeng XJ, Chen N, Li ZW, et al. Network-based algorithm for fault location with traveling wave. Proceedings of the CSEE. 2008; 28(31): 48–53. (in Chinese)
10. Chen Y, Liu D, Xu B. Wide-Area Traveling Wave Fault Location System Based on IEC61850. IEEE Transactions on Smart Grid. 2013; 4(2): 1207–1215. doi: 10.1109/TSG.2012.2233767
11. Hamidi RJ, Livani H. Traveling-Wave-Based Fault-Location Algorithm for Hybrid Multiterminal Circuits. IEEE Transactions on Power Delivery. 2017; 32(1): 135–144. doi: 10.1109/TPWRD.2016.2589265
12. Liang R, Peng N, Zhou L, et al. Fault Location Method in Power Network by Applying Accurate Information of Arrival Time Differences of Modal Traveling Waves. IEEE Transactions on Industrial Informatics. 2020; 16(5): 3124–3132. doi: 10.1109/TII.2019.2903267
13. Yu D, Zhou N, Liao J, et al. Modified VMD Algorithm-Based Fault Location Method for Overhead-Cable Hybrid Transmission Line in MTDC System. IEEE Transactions on Instrumentation and Measurement. 2024; 73: 1–11. doi: 10.1109/TIM.2024.3383458
14. Etingov D, Zhang P, Shamash YA. IoT-Enabled Traveling Wave Microgrid Protection. IEEE Internet of Things Journal. 2025; 12(7): 9169–9179. doi: 10.1109/JIOT.2024.3506559
15. Xie L, Luo L, Ma J, et al. A novel fault location method for hybrid lines based on traveling wave. International Journal of Electrical Power & Energy Systems. 2022; 141: 108102. doi: 10.1016/j.ijepes.2022.108102
16. Yu K, Zeng J, Zeng X, et al. A novel traveling wave fault location method for transmission network based on time linear dependence. International Journal of Electrical Power & Energy Systems. 2021; 126: 106608. doi: 10.1016/j.ijepes.2020.106608
17. Naidu O, Pradhan AK. A Traveling Wave-Based Fault Location Method Using Unsynchronized Current Measurements. IEEE Transactions on Power Delivery. 2019; 34(2): 505–513. doi: 10.1109/TPWRD.2018.2875598
18. Wu G, Li Z, Xia Y, et al. Traveling Wave Network Location Method Based on Virtual Fault Time Difference Information. IEEE Transactions on Industrial Informatics. 2025; 21(8): 5866–5876. doi: 10.1109/TII.2025.3555989
19. Zhang C, Yan J, Yang L, et al. Analysis of Traveling Wavefront Information and Wavefront Protection for Power Electronic Device-Interfaced AC System. IEEE Transactions on Power Delivery. 2024; 39(1): 407–425. doi: 10.1109/TPWRD.2023.3239877
20. Xia Y, Li Z, Xi Y, et al. Accurate Fault Location Method for Multiple Faults in Transmission Networks Using Travelling Waves. IEEE Transactions on Industrial Informatics. 2024; 20(6): 8717–8728. doi: 10.1109/TII.2024.3371998
21. Xia Y, Li Z, Xi Y, et al. Distribution Network Fault Location Method Based on Wide Scale Time Window Difference Operator. IEEE Transactions on Industrial Informatics. 2024; 20(3): 3446–3455. doi: 10.1109/TII.2023.3308340
22. Galvez C, Abur A. Fault Location in Power Networks Using a Sparse Set of Digital Fault Recorders. IEEE Transactions on Smart Grid. 2022; 13(5): 3468–3480. doi: 10.1109/TSG.2022.3168904
23. Salehi M, Akbar Motie Birjandi A, Dong X. Determining minimum number and placement of fault detectors in transmission network for fault location observability. International Journal of Electrical Power & Energy Systems. 2021; 124: 106386. doi: 10.1016/j.ijepes.2020.106386
24. Mohammadi P, Mehraeen S, Nazaripouya H. Sensitivity analysis-based optimal PMU placement for fault observability. IET Generation, Transmission & Distribution. 2021; 15(4): 737–750. doi: 10.1049/gtd2.12055
25. Dolatabadi SHH, Golshan MEH. Fault location observability rules for impedance-based fault location algorithms. Electric Power Systems Research. 2023; 224: 109771. doi: 10.1016/j.epsr.2023.109771
26. Mohammadniaei M, Namdari F, Shakarami M, et al. A novel single sensor based fault/branch location method in distribution systems based on combination of game theory and Dijkstra's algorithm. IET Generation, Transmission & Distribution. 2022; 16(21): 4433–4443. doi: 10.1049/gtd2.12612
27. Maritz ECM, Maritz JM, Salehi M. A Travelling Wave-Based Fault Location Strategy Using the Concepts

of Metric Dimension and Vertex Covers in a Graph. IEEE Access. 2021; 9: 155815–155825. doi: 10.1109/ACCESS.2021.3129736
28. Korkali M, Lev-Ari H, Abur A. Traveling-Wave-Based Fault-Location Technique for Transmission Grids via Wide-Area Synchronized Voltage Measurements. IEEE Transactions on Power Systems. 2012; 27(2): 1003–1011. doi: 10.1109/TPWRS.2011.2176351
29. Noto M, Sato H. A method for the shortest path search by extended Dijkstra algorithm. In: Proceedings of the 2000 IEEE International Conference on Systems, Man and Cybernetics; 8–11 October 2000; Nashville, TN, USA. pp. 2316–2320. doi: 10.1109/ICSMC.2000.886462
30. Palupi Rini D, Mariyam Shamsuddin S, Sophiyati Yuhaniz S. Particle Swarm Optimization: Technique, System and Challenges. International Journal of Computer Applications. 2011; 14(1): 19–27. doi: 10.5120/1810-2331
31. Liang R, Xu C, Wang F, et al. Optimal deployment of fault location devices based on wide area travelling wave information in complex power grid. Transactions of China Electrotechnical Society. 2016; 31: 30–38.
32. Fan XQ, Zhu YL, Lu WF. Traveling Wave Based Fault Location for Transmission Lines Based on EMD-TEO. Power System Protection and Control. 2012; 40(9): 8–12. (in Chinese)
33. Anane POK, Huang Q, Ayimbire PN, et al. Non-contact measurement of traveling wave of overhead transmission line. Measurement. 2021; 181: 109557. doi: 10.1016/j.measurement.2021.109557